ARCHIVES OF ACOUSTICS
36, 4, 887–900 (2011)

DOI: 10.2478/v10168-011-0059-z

Efficiency of Ultrasonic Comb Transducers

Eugeniusz J. DANICKI

Institute of Fundamental Technological Research
Polish Academy of Sciences
Pawińskiego 5B, 02-106 Warszawa, Poland
e-mail: edanicki@ippt.gov.pl

(*received February 18, 2011; accepted March 9, 2011*)

Comb transducers are applied in ultrasonic testing for generation of Rayleigh or Lamb waves by scattering of the incident bulk waves onto surface waves at the periodic comb-substrate interface. Hence the transduction efficiency, although rarely discussed in literature, is an important factor for applications determining the quality of the measured ultrasonic signals. This paper presents the full-wave theory of comb transducers concluded by evaluation of their efficiency for a couple of examples of standard and certain novel configurations.

Keywords: ultrasonic transducers, interface waves, Bragg reflection.

1. Introduction

Comb transducers (Victorov, 1967) are applied in ultrasonic testing primarily for generation of strong Rayleigh (Hurley, 1999) or Lamb (Quarry, Rose, 2002) waves by transformation of the incident bulk waves onto surface waves that takes place at the periodic comb-substrate contact. Hence the transduction efficiency, although rarely discussed in literature (Danicki, 2000), is an important factor for application, determining the quality of the measured ultrasonic signals.

A typical comb transducer is an acoustic buffer with periodic teeth carved on its surface and applied to the flat surface of a tested substrate. The sliding comb-substrate contact does not mean that the mechanical coupling between them is weak. The considered system is a quite complex, mechanical waveguide for interface waves (Danicki, 2010) which propagate under the transducer until they are converted to surface waves on the free substrate surface outside the comb.

A novel comb-like transducer is proposed here, with periodic sliding spacers between acoustic buffer and the substrate instead of teeth etched in the buffer. This idea is investigated for spacers made of different materials, particularly

plastic spacers which can better fit to the rough substrate surface in certain applications.

The considered wave phenomena includes the Bragg scattering of interface waves which evolves in periodic system of teeth or spacers. Assuming normal incidence of bulk waves propagating in the buffer onto its contact plane with the substrate, the generated interface wave-field comprises the 0th and ± 1 Bloch components, the latter two carrying acoustic power along the buffer-substrate interface (to be eventually converted into SAWs outside the transducer); the former component is responsible for specular reflection and transmission of the incident wave at the interface. The interface wave under consideration is a complex leaky wave losing its power to the semi-infinite media, the buffer and the substrate, caused by 0th Bloch order component of interface stress.

The detailed analysis of the considered boundary-value problem for the discussed interface waves is presented in earlier papers (Danicki, 2008; Besserer, Malishevsky, 2004), including impedance of teeth treated as a piece of elastic plate with its stress-free side surfaces (Fig. 1), and impedance of semi-infinite elastic substrate or buffer (without teeth). The next section presents these results briefly. The following sections present interface waves in several transducer configurations and finally, the transducer generation and detection efficiencies of surface waves in the substrate.

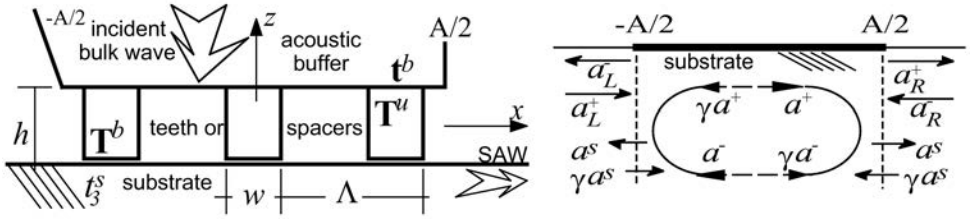

Fig. 1. Comb transducer with periodic teeth or sliding spacers inserted between the buffer and the substrate. Normal incident longitudinal wave-beam of aperture width A excites interface waves in the system, which transform into Rayleigh waves (SAW) at the comb edges in the scattering/reflection phenomenon, depicted on the right-hand side drawing.

2. The boundary-value problem

2.1. Surface mechanical fields

The harmonic wave-fields $\exp(i\omega t - ipx)$ are considered at the substrate surface and the buffer above the teeth level (Fig. 1), of height h; ω and p are temporal and spatial frequencies. The displacement vector $\mathbf{u}$ and stress tensor $\mathbf{t}$ (without y-components) will be marked by superscripts b or s, correspondingly for the buffer and the substrate surface. The corresponding fields on the upper and bottom ends of teeth are $\mathbf{U}$ and $\mathbf{T}$, with superscripts u and b, respectively.

In the substrate spanning from $z = 0$ down to $-\infty$, the normal surface traction t_{33} (denoted shortly by t^s (the other traction component $t_{31} = 0$ due to the assumed sliding contact with comb transducer) applied to the substrate surface, causes the normal surface displacement $u^s = u_3$ according to (DANICKI, 2010):

$$u^s = \frac{i}{\mu}\, g_s t^s, \qquad g_s(p) = \frac{q_t k_t^2}{(2p^2 - k_t^2)^2 + 4p^2 q_l q_t}, \tag{1}$$

where $q_{l,t} = \sqrt{k_{l,t}^2 - p^2} = -i\sqrt{p^2 - k_{l,t}^2}$, and $k_{l,t}$ are wave-numbers of longitudinal and transversal waves in an elastic body; μ is its Lamé constant.

A free Rayleigh wave (with wave-number k_R) in the substrate transports acoustic power $\Pi = |a|^2/2$ along the surface, where a is the wave amplitude depending on the surface displacement $u^s = u_3$:

$$|a|^2 = |\dot{g}_s/2|\mu_s \omega |u^s|^2, \qquad \dot{g} = dg_s^{-1}/dr\ |_{r=k_R}\ . \tag{2}$$

This dependence can be evaluated using the analysis presented in (DANICKI, 2006).

In the acoustic buffer, spanning from the teeth basis to infinity, the normal incident wave is characterized by particle displacement u_3^I and traction $t_{33}^I = t_3^I$, satisfying Eq. (1) for corresponding μ^b, $k_{l,t}^b$ of the buffer. The total displacement and traction at the buffer surface: $\mathbf{u}^b$ on $\mathbf{t}^b$, satisfy equations (DANICKI, 2010):

$$\begin{bmatrix} u_1^b \\ u_3^b \end{bmatrix} = -i\mu^{-1} \begin{bmatrix} g_1 & g_2 \\ -g_2 & g_3 \end{bmatrix} \begin{bmatrix} t_1^b \\ t_3^b \end{bmatrix} + 2 \begin{bmatrix} u_1^I \\ u_3^I \end{bmatrix},$$

$$\begin{bmatrix} g_1 & g_2 \\ -g_2 & g_3 \end{bmatrix} = \frac{\begin{bmatrix} q_l k_t^2 & -p(q_t^2 - p^2 - 2q_l q_t) \\ p(q_t^2 - p^2 - 2q_l q_t) & q_t k_t^2 \end{bmatrix}}{(2p^2 - k_t^2)^2 + 4p^2 q_l q_t}, \tag{3}$$

where u_1^I can be neglected for close to normal incidence assumed here; $q_{l,t}$ are evaluated analogously to these in Eq. (1), using corresponding μ^b, $k_{l,t}^b$.

2.2. Wave-fields at the teeth ends

A tooth of width w and height h (Fig. 1) has its side surfaces stress-free. Its end surfaces at $z = \pm h/2$ respond with displacements $U_i(x)|_{z=\pm h/2}$ to the loading stress $T_{3j}(x)|_{z=\pm h/2} = T_j$ $(i, j = 1, 3$; capital letters are used for wave-fields in the teeth). These surface wave-fields are expanded in natural Fourier series over the domain $(-w/2, w/2)$, that is (the column matrix $\mathbf{F}$ is truncated to proper dimension determining numerical accuracy):

$$F(x) = \mathrm{diag}\{\exp(-inWx)\}\mathbf{F}, \qquad W = 2\pi/w, \qquad n \in [-N, N]. \tag{4}$$

The dependence of U_i on T_j expanded correspondingly in the harmonic series results from the intrinsic dynamics of the strip. The modal expansion analysis of the wave-field in teeth yields the following dependence of interest:

$$\begin{bmatrix} \mathbf{U}_1^u \\ \mathbf{U}_3^u \\ \mathbf{U}_3^b \end{bmatrix} = \frac{-i}{\mu} \begin{bmatrix} \mathbf{A} & \mathbf{B} & \mathbf{a} & \mathbf{b} \\ \mathbf{C} & \mathbf{D} & \mathbf{c} & \mathbf{d} \\ \mathbf{c} & -\mathbf{d} & \mathbf{C} & -\mathbf{D} \end{bmatrix} \begin{bmatrix} \mathbf{T}_1^u \\ \mathbf{T}_3^u \\ \mathbf{T}_3^b \end{bmatrix}, \tag{5}$$

including its symmetry properties (for isotropic teeth), where the matrix components are evaluated numerically using the method presented in (Danicki, 2010). Note that we neglected $T_1^b(x) = 0$ at the sliding comb-substrate contact, hence $U_1^b(x)$ is not included in the above equation. The included matrix vectors $\mathbf{U}_i$, $\mathbf{T}_1$ are the components of natural Fourier series (with expansion domain over the strip width w) of the corresponding wave-field.

The above matrix components present the dependence of particular components of displacements on particular components of traction. For example, $\mathbf{A}$ is involved in relation of harmonic components of displacement u_1 at the upper side of the strip on the traction T_{31} applied to the same strip side, while the matrix $\mathbf{c}$ yields the displacement u_3 on the other side of strip resulting from this traction. Analogously other components, with capital letters ($\mathbf{A}$, $\mathbf{B}$, $\mathbf{C}$, $\mathbf{D}$) concerning displacements and stresses on the same strip ends, while the normal letters ($\mathbf{a}$, $\mathbf{b}$, $\mathbf{c}$, $\mathbf{d}$) – on the other strip sides. Generally, these particular matrices, when multiplied by ω/μ, can be called the particular harmonic trans-impedances of elastic strips.

2.3. The scattering problem

Due to the periodicity of the system of teeth, the wave-fields at their contact planes with acoustic buffer or the substrate is searched in the form of Bloch expansion:

$$f(x) = \sum_{k=-M}^{M} f^{(k)} e^{-i(r+kK)x} = \mathrm{diag}\{e^{-i(r+kK)x}\}\mathbf{f}, \tag{6}$$

where Λ is the period of teeth, $K = 2\pi/\Lambda$, and $r \in (-K/2, K/2)$ is the reduced wave-number belonging to the first Brillouin zone; it is the x-projection of the incident wave on the contact plane: $\exp(-ipx)$, $p = r \approx 0$. The data vector describing the incident wave by its Bloch expansion $\mathbf{u}^I(p)$ has only one nonzero component u^I in $M{+}1$ row of the corresponding matrix.

Similar form of Bloch expansion is applied for fields at the substrate surface u_3^s, t_3^s, and the buffer surface u_i^b, t_j^b, $i, j = 1, 3$. Note that their Bloch components, having the wave-number $p = r + nK$, are governed by Eqs. (1) and (3):

$$\mathbf{u}_k^b = \mathbf{g}_b(r + kK)\mathbf{t}_k^b + 2\mathbf{u}^I, \qquad u_k^s = -g_s(r + kK)t_k^s. \tag{7}$$

In the discussed problem, the particle displacements continuity is required at the contact domains of teeth with the substrate or buffer, $x \in (-w/2, w/2) + l\Lambda$ (l – arbitrary integer). The surface traction on the teeth ends must be equal to that on the substrate and buffer. Note however that the traction between teeth vanish. Hence, using the field expansion of Eqs. (4) and (6), the boundary conditions are:

$$\begin{aligned} &\mathrm{diag}\{e^{-inWx}\}\mathbf{U}^{\mathrm{T}}_{u,b} = \mathrm{diag}\{e^{-i(r+kK)x}\}\mathbf{u}^{\mathrm{T}}_{u,b}, \quad \text{for } \; x \in (-w/2, w/2) + l\Lambda, \\ &\mathrm{diag}\{e^{-i(r+kK)x}\}\mathbf{t}^{\mathrm{T}}_{u,b} = \mathrm{diag}\{e^{-inWx}\}\mathbf{T}^{\mathrm{T}}_{u,b}, \qquad \text{for} \begin{cases} x \in (-w/2, w/2) + l\Lambda, \\ \text{otherwise zero.} \end{cases} \end{aligned} \tag{8}$$

Applying Fourier integration over $x \in (-w/2, w/2)$, yields (Danicki, 2008):

$$\begin{gathered} \mathbf{U}^{u,b}_i = \mathbf{V}\mathbf{u}^{b,s}_i, \qquad \mathbf{t}^{b,s}_j = \beta\mathbf{V}^{\mathrm{T}}\mathbf{T}^{u,b}_j, \\ \mathbf{V} = \left[\frac{\sin\{(r+kK)w/2 - n\pi\}}{(r+kK)w/2 - n\pi}\right], \qquad \beta = K/W, \qquad \beta\mathbf{V}^{\mathrm{T}}\mathbf{V} \approx \mathbf{I}, \end{gathered} \tag{9}$$

where $\mathbf{I}$ is a unitary matrix of corresponding dimension. The above, Eqs. (7) and (3), constitute the scattering problem under consideration ($\overline{\mathbf{g}}_s = \beta\mathbf{V}\mathbf{g}_s\mathbf{V}^{\mathrm{T}}$):

$$\begin{aligned} \mathbf{A}\mathbf{T}^u_1 + \mathbf{B}\mathbf{T}^u_3 + \mathbf{b}\mathbf{T}^b_3 &= o_b(\overline{\mathbf{g}}_1\mathbf{T}^u_1 + \overline{\mathbf{g}}_2\mathbf{T}^u_3 + 2\mathbf{V}\mathbf{u}^I_1), \\ \mathbf{C}\mathbf{T}^u_1 + \mathbf{D}\mathbf{T}^u_3 + \mathbf{d}\mathbf{T}^b_3 &= o_b(-\overline{\mathbf{g}}_2\mathbf{T}^u_1 + \overline{\mathbf{g}}_3\mathbf{T}^u_3 + 2\mathbf{V}\mathbf{u}^I_3), \\ \mathbf{c}\mathbf{T}^u_1 - \mathbf{d}\mathbf{T}^u_3 - \mathbf{D}\mathbf{T}^b_3 &= o_s(-\overline{\mathbf{g}}_s\mathbf{T}^b_3), \qquad \overline{\mathbf{g}}_i = \beta\mathbf{V}\mathbf{g}_i\mathbf{V}^{\mathrm{T}}, \end{aligned} \tag{10}$$

where $o_b = \mu_t/\mu_b$, $o_s = \mu_t/\mu_s$; μ_t, μ_b and μ_s are the Lamé constants of teeth, buffer and substrate, respectively, and g_i characterize the buffer, Eqs. (3).

3. Interface wave-modes

3.1. Propagation

The nontrivial solution to Eqs. (10) for $u^I = 0$ at certain $r = \pm r_o$ is the interface wave propagating freely at the comb-substrate interface. We are interested most in the solution for $\mathbf{u}^s$ which can be obtained from $\mathbf{T}^b_3$ by subsequent applications of Eqs. (9) and (1). The most important components of the Bloch expansion $\mathbf{u}^s$ are these associated with wave-numbers $r_o \pm K$ which are close to $\pm k_R$, hence they transport the acoustic power along the substrate surface as presented in Eq. (2). The 0th Bloch component with wave-number $r_o = r_R + ir_I$ is responsible for the interface wave leakage into bulk waves in the substrate and buffer (what causes r_o to be complex-valued; we apply $r_I > 0$ by definition). Other Bloch components represent localized vibrations at the teeth edges which are not discussed here.

It is convenient to introduce the coefficients:

$$\gamma_{\pm 1} = u^{(\pm 1)}/u^{(0)}, \qquad \gamma = u^{(+1)}/u^{(-1)}, \tag{11}$$

where $u^{(\pm 1,0)} = [\mathbf{u}^s]^{(\pm 1,0)}$ are Bloch components corresponding to the wave-numbers $r_o \pm K, r_o$; they are called the forward and backward waves, respectively. The coefficient $\gamma = \gamma_1/\gamma_{-1}$ is called the standing wave coefficient for the wave propagating to the left and decaying at $x \to -\infty$ when $r_I = \mathrm{Im}\{r_o\} > 0$, what is the case of the following discussion (there is also a solution at $-r_o$ for the wave propagating to the right).

It is evident from Eq. (2) that the -1st Bloch component transports acoustic power to the left (because $r_o - K < 0$) and the $+1$st component transports the power to the right. Only certain imbalance of these powers caused by the difference between $r_o \pm K$ and by $|\gamma| < 1$ makes the net power transportation to the left by this complex wave in the periodic system of teeth. The forward component of interface wave carries the power in the same direction by definition. Accordingly, for the right propagating interface waves with wave-number $-r_o$, $|u^{(-1)}/u^{(+1)}| > 1$.

In some cases however, particularly for asymmetric systems including combs, the net power in the substrate (analyzed in this paper) and the net power in the buffer can be transported in different directions. When the net power in the buffer is larger than that in the substrate, it may result in $|\gamma| > 1$ *in spite of* $Im\{r_o\} > 0$. *Deeper discussion of this wave phenomena (*Luisell*, 1960) is far beyond the scope of this paper.*

In periodic systems, r_o takes complex value in stopband domain of wave-number K (say between K_1 and K_2, which are called the stopband edges) due to the Bragg reflections. This phenomenon is also observed for the discussed leaky interface waves where the wave-number behaves like:

$$r_o^2 \approx (K - K_1)(K - K_2) + \text{imaginary part caused by leakage;} \tag{12}$$

$|\gamma| = 1$ in the stopband results from the energy conservation law in ideal case without leakage, because the ideal standing wave does not transport power along the substrate surface. In this paper we consider combs with teeth period close to the surface wavelength: $K \approx k_R$ resides in or close to the domain (K_1, K_2), hence $r_o \approx 0$.

3.2. Generation

The above discussion helps us to evaluate the power transformation of the incident bulk wave in the buffer into the interface wave propagating along the substrate toward the comb edges, where it is converted to the Rayleigh waves on the free substrate surface. The solution to Eqs. (10) for $u^{(0)}$ exhibits a pole at r_o, hence it is a function of r like:

$$u^{(0)}(r) = u^I R/(r^2 - r_o^2), \qquad u^I = u_3^I, \tag{13}$$

where $1/R$ can be evaluated by numerical differentiation of $u^I/u^{(0)}$ with respect to r^2 at r_o. It depends on the incident wave amplitude u^I which, being the spatial spectrum of a finite incident wave-beam, is also a function of r.

The spatial solution, having the form of an outgoing wave $u_0 \exp(-irx)$, is the corresponding inverse Fourier transform:

$$u^{(0)}(x<0) = \frac{1}{2\pi} \int_{-K/2}^{K/2} u^{(0)}(r) e^{-irx}\,\mathrm{d}r \approx u_0 e^{\mp ir_o x}, \qquad u_0 = \frac{iR}{2r_o}\,u^I, \tag{14}$$

integration of which can be extended to infinity if allowed by the Cauchy condition. In our case, this only requires x to reside outside the domain of the incident wave-beam (outside the comb area). Indeed, for comb comprising many teeth, the spatial spectrum of incident wave-beam is well confined within the domain $(-K/2, K/2)$, hence extending of the integration limits is acceptable.

The corresponding forward and backward waves propagating in the substrate have wave-numbers $r_o \pm K$ and amplitudes $u^{(\pm 1)} = \gamma_{\pm 1} u_0$. On the left-hand side of the incident wave-beam, they are:

$$u_0[\gamma_{-1} e^{iKx} + 1 + \gamma_{+1} e^{-iKx}] e^{-ir_o x}, \qquad x < -A/2, \tag{15}$$

where A is the incident wave-beam aperture width. They carry acoustic power to the left and to the right along the substrate surface, and according to Eq. (2), their amplitudes are $a_s = (|\dot{g}_s/2|\mu_s\omega)^{1/2} u^{(-1)}$ and γa_s, respectively, because in the stopband where $r_R = 0$, $\dot{g}_s$ evaluated at $r_R \pm K \approx K \approx k_R$, are equal; we apply this approximation in order to avoid further complication of the analysis.

The interface wave-field extends also into the buffer, with displacements $u^{s(\pm 1)}$ and the forward wave amplitude a_b. The full power carried by the interface forward wave is thus $|a|^2/2 = (|a_s|^2 + |a_b|^2)/2 = |a_s|^2(1 + |\tau|^2)/2$ where $\tau = a_b/a_s$. The backward wave carries power $|\gamma a|^2/2$. Below, we apply $\tau = 1$ in order to simplify the analysis, hence $a \approx a_s\sqrt{2}$.

Due to the symmetry of the considered system and normal wave incidence, the same interface wave amplitudes and powers appear for $x > A/2$, with power $|a_s|^2/2$ transported to the right by the corresponding forward wave, and $|\gamma a_s|^2/2$ – to the left by the backward wave. Summarizing, the generated wave-fields at $x = \pm A/2$ in the substrate are correspondingly:

$$a_s e^{i(r_o - K)A/2} \quad \text{and} \quad \gamma a_s e^{i(r_o + K)A/2}.$$

4. The transducer efficiency

Inside the comb area $|x| < A/2$, free propagating interface waves with wave-numbers $\pm r_o$ exist in the substrate: $a^{\mp} \exp(\pm i(r_o - K)x)$, $\gamma a^{\mp} \exp(\pm i(r_o + K)x)$. Outside the comb area, $|x| > A/2$, the Rayleigh waves propagate to the left or

to the right in the substrate: $a_L^{\mp}\exp(\pm ik_R x)$, $x < -A/2$, and $a_R^{\pm}\exp(\mp ik_R x)$, $x > A/2$. Here we assume that the forward, backward and Rayleigh waves have all similar modal profiles according to the earlier assumption that $r_o \approx 0$ and $K \approx k_R$. This enables us to neglect the scattering into bulk waves and to apply the following conservative boundary conditions at $x = -A/2$ (FIELD *et al.*, 1975):

$$\begin{aligned} a_s e^{i(r_o-K)A/2} + a^- e^{i(r_o-K)A/2} + \gamma a^+ e^{i(r_o+K)A/2} &= a_L^- e^{-ik_R A/2}, \\ \gamma a_s e^{i(r_o+K)A/2} + \gamma a^- e^{i(r_o+K)A/2} + a^+ e^{i(r_o-K)A/2} &= a_L^+ e^{ik_R A/2}/\sqrt{2}; \end{aligned} \tag{16}$$

the conditions at $x = A/2$ are similar; one needs only to replace superscripts $+, -$ by $-.+$ and subscripts L, R by R, L.

The right-hand sides of the above equations require further explanations. For an incident surface wave in the substrate, carrying power $|a_L^+|^2/2$ toward the transducer area, we must first decompose it into waves in both the substrate and the buffer, in order to obtain the wave-mode shape matching the shape of the interface wave. In our case, this matched wave amplitude is a' in the substrate and $\pm\tau a'$ in the buffer, carrying together the power of the incident wave, hence $a_L^+/\sqrt{1+\tau^2} \approx a_L^+/\sqrt{2}$ is the incident wave amplitude applied in the second row of Eqs. (16). Note that only one of the above discussed pairs of modes is matched to the interface wave, the other one (below referred to as RM) is entirely reflected from the comb edge.

Evaluation of the free interface waves $a^{\pm}$ bouncing between the comb edges, yields the generated Rayleigh wave amplitude at the left-hand side of the comb:

$$a_L^- = \frac{R}{2}\frac{\gamma_{-1}}{r_o} u^I(r_o) k_t \sqrt{\mu\omega|\dot{g}_s|/2}\,\frac{1+\gamma}{1+\gamma e^{ir_o A}}\, e^{ir_o A/2} \tag{17}$$

(for $K \approx k_R$), where $u^I(r)$ is the spatial spectrum of uniform normal incident wave-beam of aperture width A and displacement amplitude u^I:

$$u^I(r) = 2u^I \sin(rA/2)/r, \tag{18}$$

and $\dot{g}_s$ is evaluated from Eq. (2) at $|r_o - K| \approx k_R$.

The incident power is $P^I = AZ_l^b|\omega u^I|^2/2$, where $Z_l^b = \rho^b\omega/k_l^b$ is the acoustic impedance of the buffer for longitudinal waves. For small r_o residing in the stopband where $r_R \approx 0$, the comb transducer generation efficiency is:

$$\eta_g = \sqrt{\frac{|a_L^-|^2}{2P^I}} = \left|\frac{R\gamma_{-1}}{4r_o}\right| \left|\frac{k_t^s}{k_t^b}\right| \left|\frac{(1-e^{ir_o A})(1+\gamma)}{r_o A(1+\gamma e^{ir_o A})}\right| \sqrt{k_l^b A|\dot{g}_s|/o_s}. \tag{19}$$

The generated Rayleigh wave to the right of the comb has similar amplitude if $r_o \approx 0$, but it can be different for off-normal incident wave. This case will not be discussed here.

The Eqs. (16) also yields the solution to the classic scattering problem for evaluation of the outgoing Rayleigh waves a_L^-, a_R^+, dependent on the incident surface wave a_L^+, for instance (for $\tau = 1$):

$$a_L^- = \frac{a_L^+}{\sqrt{2}} \frac{\gamma(1 - e^{i2r_oA})}{1 - \gamma^2 e^{i2r_oA}}, \qquad a_R^+ = \frac{a_L^+}{\sqrt{2}} \frac{(1 - \gamma^2)e^{ir_oA}}{1 - \gamma^2 e^{i2r_oA}}. \tag{20}$$

For large A, the reflected SAW amplitude at the left-hand edge of the comb $|a_L^-|$ equals $|\gamma a_L^+|$ (note that $\exp(ir_oA)$ vanishes for the chosen values of $r_I > 0$ and $A \to \infty$); $|a_R^+|$ is the transmitted SAW amplitude at the right-hand comb edge. Hence γ is the reflection coefficient from a semi-infinite system of periodic teeth.

Comparing the incident SAW power $|a_L|^2/4$ (neglecting RM) with the reflected and transmitted wave powers $|a_L^-|/2 + |a_R^+|^2/2$, we notice certain imbalance resulting from the power leakage into the bulk waves (mostly longitudinal) in the substrate. According to the earlier assumption, the same waves propagate in the buffer and they can be detected by a piezoelectric transducer on the other end of the buffer. Hence, this power imbalance is a signature of the receiving comb efficiency of transformation of the incident SAWs into bulk waves to be detected. Summarizing, the approximation for the square of the transducer efficiency is (accounting for the lost RM):

$$1/2 - |a_L^-/a_L^+|^2 - |a_R^+/a_L^+|^2,$$

which limit at $A \to \infty$ is $\eta_r^2 \to (1 - |\gamma|^2)/2$.

It must be noted however that the flat receiving piezoelectric transducer placed on the upper end of the acoustic buffer, averages the wave of variable phase. The signal produced by transducer of aperture A is proportional to:

$$\int_{-A/2}^{A/2} a^- e^{-ir_o(x+A/2)}\,\mathrm{d}x + \int_{-A/2}^{A/2} a^+ e^{ir_o(x-A/2)}\,\mathrm{d}x = (a^- + a^+)\frac{1 - e^{ir_oA}}{r_o},$$

which, for small r_o, is $(a^- + a^+)A$. Hence the relative effect of the signal averaging by the flat receiving transducer can be estimated by $[1 - \exp(ir_oA)]/(r_oA)$. The corrected transducer efficiency

$$\eta_r = \left|\frac{1 - \exp(ir_oA)}{r_oA}\right| \sqrt{1/2 - |a_L^-/a_L^+|^2 - |a_R^+/a_L^+|^2}, \tag{21}$$

accounts for the off-normal propagation of the incident bulk waves onto the receiving piezoelectric transducer placed on top of the acoustic buffer.

5. Numerical examples

5.1. Aluminium comb applied to steel substrate

In numerical examples presented below, we applied for aluminium: $\mu^{\mathrm{Al}} = 25$ [10^9 Nm^{-2}], $\overline{k}_l^{\mathrm{Al}} = 0.1558$, $\overline{k}_t^{\mathrm{Al}} = 0.3283$ and the Rayleigh wave-number $\overline{k}_R^{\mathrm{Al}} = 0.3509$, all in units [mm^{-1}], where $\overline{k} = k/2\pi$. The width of teeth was chosen $w = 0.48/\overline{k}_R^{\mathrm{Al}}$, that is about half-wavelength of the Rayleigh wave in aluminium. The parameters of steel are: $\mu^{\mathrm{Fe}} = 82$, $\overline{k}_l^{\mathrm{Fe}} = 0.1686$, $\overline{k}_t^{\mathrm{Fe}} = 0.3098$, and $\overline{k}_R^{\mathrm{Fe}} = 0.3346$, in the same units.

In the first example, the comb having teeth of height $h = 1.05w$ carved in an aluminium buffer is applied to steel substrate with sliding contact; hence all the above equations, particularly Eq. (10) (with $o_b = 1$), matter for the considered scattering problem. Figure 2 presents the pseudo-dispersive curve r_o^2 *vs.* K (for constant ω) and the standing wave coefficient $|\gamma|$. We notice that there is a narrow domain of K for which $\mathrm{Re}\{r_o^2\} < 0$ what, neglecting small $\mathrm{Im}\{r_o^2\}$, results in imaginary r_o being the signature of stopband.

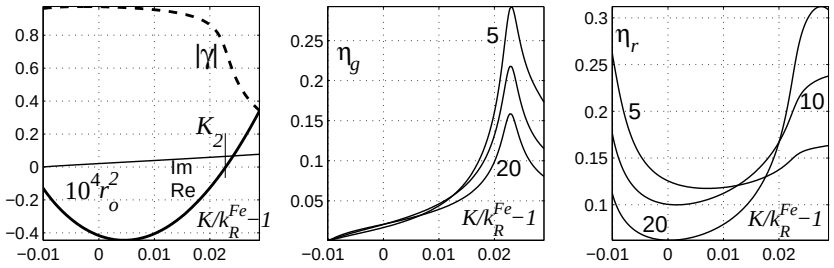

Fig. 2. Aluminium comb on steel substrate: characterization of interface waves ($r_o^2, |\gamma|$ *vs.* K), and the transducer efficiencies η_r, η_g for different number of teeth in the comb, $N = 5, 10, 20$.

It is important that the considered stopband (in the K-domain) resides above the cut-off wave-numbers of bulk waves of both the buffer and the substrate (above k_t^b and k_t^s), hence the leakage mechanism of the interface waves in the considered system is provided only by 0th Bloch interfacial wave-field, producing almost normal outgoing bulk waves in the comb and in the substrate.

Analogous results are presented in Fig. 3 for aluminium comb on aluminium substrate, for the teeth height equal to $h = 3.3w$. In this case, the leakage phenomenon is much stronger (higher imaginary values of r_o^2), and the receiving efficiency η_r in stopband is slightly higher when compared to the previous example, but the generation efficiency is much smaller, what is a quite unexpected result. It proves that the comb transducers are rather a difficult device for optimization.

Occasionally, the comb transducers may be applied for generation of strong surface waves. In this case, more important is the total power $A\eta_g^2$ of the excited

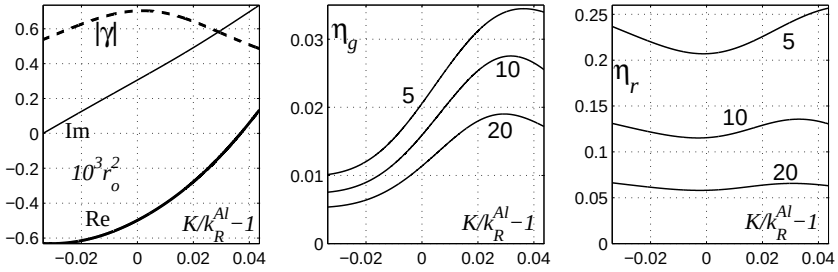

Fig. 3. Aluminium comb with $5, 10, 20$ teeth on aluminium substrate: $r_o^2, |\gamma|$ and η_r, η_g.

wave than the transducer efficiency. Figure 4 presents this parameters for the comb on steel (ref. Fig. 2), for two values of K: in the center of the stopband and at its right-hand edge K_2. As expected, the latter is much higher, resulting from larger η_g and small wave damping (small imaginary part of r_o), allowing many teeth to contribute to the output power.

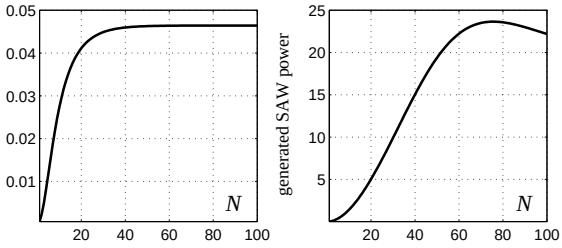

Fig. 4. Al comb on steel substrate: the dependence of the generated SAW power for K chosen at stopband center (left) and at the stopband edge K_2 (right) on teeth number N.

The maximum generated power decreases above the stopband edge K_2 due to the lack of synchronism between the surface wave-field excited by periodic teeth insonified by the normal incident wave $\exp(\pm iKx)$ and the propagating interface wave, the phase of which varies according to $\exp(-i(r_o \pm K)x)$. This shows that the performance of combs with off-normal incident wave properly chosen to maintain the wave synchronism, may be much better (albeit impractical for many experimental cases as compared to ordinary wedge transducers).

5.2. Sliding periodic spacers

For the case of sliding teeth, the Eqs. (10) simplify much because $\mathbf{T}_1^u$ vanishes, yielding:

$$\begin{aligned} (\mathbf{D} - o_b\overline{\mathbf{g}}_3)\mathbf{T}_3^u + \mathbf{d}\mathbf{T}_3^b &= o_b 2\mathbf{V}\mathbf{u}_3^I, \\ \mathbf{d}\mathbf{T}_3^u + (\mathbf{D} - \mathbf{o_s}\overline{\mathbf{g}}_\mathbf{s})\mathbf{T}_3^b &= \mathbf{0}. \end{aligned} \tag{22}$$

The considered examples below concern symmetric structures: the sliding teeth are applied between a pair of elastic half-spaces of the same materials, which are aluminium or steel. The teeth are either from aluminium or nylon (which material constants are: $\mu^t = 1.8$, $\overline{k}_l^t = 0.4733$, $\overline{k}_t^t = 0.7888$, in the same units).

Figures 5 present results for aluminium spacers of height $h = 2w$ between steel buffer and substrate (which value yields the wide stopband). Again, there is a maximum efficiency at the stopband edge K_2. The last Figs. 6 concern the nylon spacers between aluminium buffer and substrate; it is an experimentally promising configuration as the plastic spacers easily fit rough substrate surface. In this case the dependence of the transducer efficiency on K is relatively smooth in the stopband, but its value is not high. In all the presented cases the efficiency of the receiving transducer, as defined by Eq. (21), is higher than the generating ones. Note however that this analysis does not include the efficiency of the piezoelectric transducers converting ultrasonic waves into electric signal and *vice versa*.

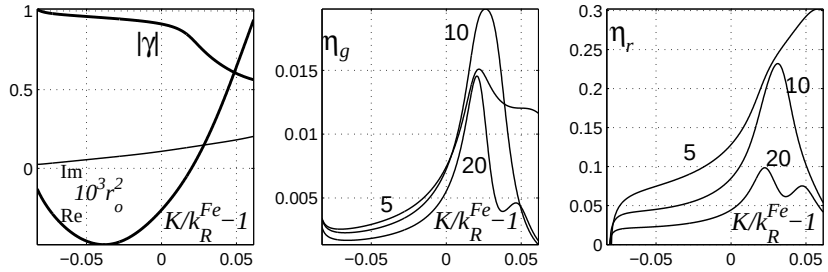

Fig. 5. The results for aluminium spacers of $2w$ height between steel buffer and substrate.

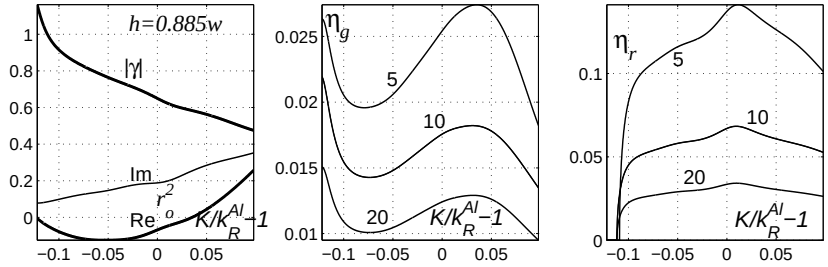

Fig. 6. Promising configuration of nylon spacers between the aluminium buffer and substrate.

6. Conclusions

The evaluated properties of comb transducers are rather unexpected: the simple perturbation theory assuming weak mechanical interaction between comb teeth and the substrate would yield the maximum efficiency in the stopband. Our

results show that this is not, in general, true. Moreover, the results show that the best efficiency of comb transducers are obtained for small number of teeth, what also contradicts the expectation based on the perturbation theory (some researchers mistake the maximum generated surface waves with efficiency defined earlier in this paper).

Concluding, the comb transducers are difficult for optimization, what may be the reason of their infrequent applications in ultrasonic measurement systems. In spite of this, an interesting multi-parameter theoretical problem arises in the analysis of such mechanical structures, being certain generalization of the system of cracks analyzed in (Every, 2008; Danicki, 1999), where complex interaction takes place at the periodic interface between elastic media. Such structures are considered for application in certain electronic systems (Darinskii, Weihnacht, 2004). Another application may concern active damping of vibration of certain structures (Zou, Crocker, 2009).

Acknowledgments

The author is indebted to Mrs. Joanna Żychowicz–Pokulniewicz for helpful editorial comments that greatly improved the text of this paper.

References

1. Besserer H., Malishevsky P.S. (2004), *Mode Series Expansion at Vertical Boundaries in Elastic Waveguides*, Wave Motion, **39**, 41–59.
2. Danicki E.J. (1999), *Resonant phenomena in bulk-wave scattering by in-plane periodic cracks*, J. Acoust. Soc. Am., **105**, 84–92.
3. Danicki E. (2000), *Periodic Crack-Model of Comb Transducers: Efficiency and Optimization*, Archives of Acoustics, **25**, 4, 487–507.
4. Danicki E.J. (2006), *Spectral Theory of Interdigital Transducers of Surface Acoustic Waves*, http://www.ippt.gov.pl/∼edanicki/danickibook.pdf, Chapt. 4.
5. Danicki E.J. (2008), *Evaluation of Planar Harmonic Impedance for Periodic Elastic Strips of Rectangular Cross Section by Plate Mode Expansion*, ASME J. Appl. Mech., **75**, 041011-1–6.
6. Danicki E.J. (2010), *Interface wave-modes in comb transducers*, Wave Motion, **47**, 508–518.
7. Darinskii A.N., Weihnacht M. (2004), *Super high-velocity leaky waves guided by a layer inserted into piezoelectric crystals*, Wave Motion, **39**, 181–190.
8. Every A.G. (2008), *Guided Elastic Waves at a Periodic Array of Thin Coplanar Cavities in a Solid*, Phys. Rev. B, **78**, 174104-1–11.
9. Field M.E., Ho R.C., Chen C.L. (1975), *Surface acoustic wave grating reflector*, IEEE Ultras. Symp. Proc., 430–433.

10. Hurley D.C. (1999), *Nonlinear Propagation of Narrow-Band Rayleigh Waves Excited by a Comb Transducer*, J. Acoust. Soc. Am., **106**, 1782–1788.

11. Luisell W.H. (1960), *Coupled mode and parametric electronics*, J. Willey & Sons, New York, Chapt. 3.

12. Quarry M.J., Rose J.L. (2002), *Phase Velocity Spectrum Analysis for a Time Delay Comb Transducer for Guided Wave Mode Excitation*, Lawrence Livermore Nat. Lab., Preprint UCRL-JC-138500.

13. Victorov I.A. (1967), *Rayleigh and Lamb Waves: Physical Theory and Applications*, Plenum Press, New York.

14. Zou D., Crocker M.J. (2009), *Response of a plate to PZT actuators*, Archives of Acoustics, **34**, 1, 13–23.